Correlated-interfacial-roughness anisotropy in $Si_{1-x}Ge_x$/Si superlattices

Y. H. Phang, C. Teichert, and M. G. Lagally
University of Wisconsin–Madison, Madison, Wisconsin 53706

L. J. Peticolos and J. C. Bean
AT&T Bell Laboratories, Murray Hill, New Jersey 07974

E. Kasper
Department of Physics, Universität Stuttgart, D-70174 Stuttgart, Germany
(Received 18 November 1993; revised manuscript received 4 May 1994)

Interfacial roughness in $Si_{1-x}Ge_x$/Si superlattices grown by molecular-beam epitaxy on vicinal Si(001) surfaces has been investigated using low-angle x-ray-diffraction diffuse-intensity measurements and atomic-force microscopy. The vertically correlated-interfacial roughness is, in specific situations, highly anisotropic and oriented with respect to the substrate miscut. The lateral length scale of the roughness is many times greater than the average separation of the substrate steps. The presence of the anisotropy depends on Ge concentration. A thermodynamic model for the interface morphology is presented.

I. INTRODUCTION

Growth of $Si_{1-x}Ge_x$/Si heterostructures with varying compositions and layer thicknesses provides an opportunity to tailor electronic and optical properties through strain-, symmetry-, and dimension-induced energy-band-structure change. As examples, $Si_{1-x}Ge_x$/Si-based long-wavelength infrared detectors[1] and high-speed field-effect transistors[2] have recently been demonstrated. These developments increase the potential of silicon as a material for device applications in optoelectronics and high-speed electronics. More importantly, they open the possibility of monolithic integration with Si technology.

Structural perfection is essential for optimum performance of heterostructures. Atomic arrangements in the bulk and at interfaces are determined by the competition between kinetics and thermodynamics during growth.[3] Growth of $Si_{1-x}Ge_x$/Si heterostructures on Si substrates can result in different types of imperfections. Long-range ordering of $Si_{1-x}Ge_x$,[4–6] segregation of Ge to the growth front,[7] formation of three-dimensional (3D) structures,[8,9] generation of dislocations,[10] $(2\times n)$ surface reconstruction,[9] and formation of wavy interfaces (both growth front and buried)[11–13] have been observed. An accurate picture of imperfections resulting from growth of lattice-mismatched films provides information about the underlying atomic mechanisms as well as input into understanding the electronic and optical properties of such films.

Interfacial roughness is one form of disorder that is present in all multilayer films.[14,15] Roughness of differing length scales affects the performance of heterostructures differently.[16] Several techniques[7,10,17–21] have been used to characterize $Si_{1-x}Ge_x$/Si interfacial morphology. Each is sensitive to roughness of a certain length scale. In this work, we use low-angle x-ray-diffraction (XRD) diffuse-intensity measurements[22] (which are sensitive to the widest length scale of all the techniques that have been used) to investigate interfacial roughness in $Si_{1-x}Ge_x$/Si superlattices grown on vicinal Si(001). We find that, for a range of well-defined conditions, the vertically correlated interfacial roughness is highly anisotropic. We show direct experimental evidence that the correlated-interfacial-roughness anisotropy is not arbitrarily oriented but is aligned with respect to the substrate miscut direction, which we measure independently. The lateral length scale of the roughness is, however, many times greater than the average separation of the substrate steps, thus showing that it is not caused by the replication of monatomic steps with an average separation determined by the substrate miscut angle, as has been suggested.[23,24] We also demonstrate that this correlated-roughness anisotropy is not caused by step bunching during the growth of the Si buffer layer.[12] The existence of anisotropy in the correlated roughness depends on the Ge concentration in the $Si_{1-x}Ge_x$ layers.

In addition to the diffuse XRD measurements, we use atomic-force microscopy (AFM) to investigate the outer-surface morphology of the multilayer films. The AFM measurements are consistent with the XRD results. When the XRD diffuse intensity shows that correlated-interfacial-roughness anisotropy is present, the surface shows strong anisotropic ripples. When XRD indicates no correlated roughness, AFM shows the outer-layer surface roughness to be random and small.

II. EXPERIMENT

A. Sample description

The samples used in this study are device-quality $Si_{1-x}Ge_x$/Si superlattices grown by molecular-beam epitaxy (MBE) on vicinal 4-in Si(001) substrates. Most of the samples were made in the following manner. On a

single 4-in Si wafer, three multilayers of similar structure and composition but having a different number of bilayers are grown by moving a slit over the substrate once the required number of bilayers is grown. The vacuum is maintained and the growth is not interrupted. Each wafer has regions with 10, 20, and 40 bilayers grown on it; the films are otherwise nominally identical. A total of four such wafers were fabricated, giving a matrix of 12 multilayer films that differed in layer number, alloy composition ($0.3 \leq x_{\text{nominal}} \leq 0.5$), and growth temperature ($550\,^{\circ}\text{C} \leq T \leq 600\,^{\circ}\text{C}$). The deposition rates (0.82Å and 1.07–1.71 Å/sec for the growth of the alloy layers and Si layers, respectively) are conventional for high-quality films.[10] Before deposition of the multilayers, 1000 Å Si buffer layers were grown in two stages: the first 500 Å at a temperature 50 °C higher than the multilayer growth temperature, and the subsequent 500 Å at the multilayer growth temperature. The deposition rate is 1.07–1.71 Å/sec for the growth of the buffer layers. The final layer is 100 Å of Si. We have investigated samples with different numbers of bilayers, different Ge concentrations, and different growth temperatures. We have also compared spots on the same wafers separated by large distances, and found variation in layer thickness ($d_{\text{bilayer}} \pm 5\%$) and alloy composition ($x_{\text{average}} \pm 7\%$) that we attribute to nonuniformity in the fluxes.

In addition to the above set of samples, which all had a Ge alloy layer, we investigated multilayer samples with pure Ge layers. These of necessity have to be much thinner, as pure Ge begins to grow 3D after a few monolayers.[9] The samples were grown at much lower temperatures (320 °C) and growth rates. A Si buffer layer was

TABLE I. The structures and growth conditions of samples A, B, and C. The $Si/Si_{1-x}Ge_x$ superlattices are grown on vicinal Si(001) substrates by molecular-beam epitaxy. The nominal and the measured values are indicated by *N* and *M*, respectively. χ and ϕ, respectively, are the polar angle [between normals of the sample surface and the substrate (001) planes] and azimuthal angle (in the (001) plane between the [110] direction and the direction of the miscut), completely specifying the substrate miscut. Layer thicknesses are determined from fitting the intensity distribution along the superlattice rod [i.e., $(\theta, 2\theta)$ scans]. For sample C, because the layers are so thin, the uncertainty in determining the individual layer thicknesses is larger than the nominal alloy layer thickness and is therefore not quoted. The vertical strain is determined from the separation between the Si(004) peak (from the substrate) and the superlattice peaks in its vicinity. The Ge concentrations (x) in the alloy layers are determined from the vertical strain assuming coherent strain. The Ge concentrations determined in this way are lower limits of the actual concentrations. The discrepancy between the nominal and measured concentrations indicates that the layers are not completely relaxed. Samples B and C show anisotropic long-wavelength correlated interfacial roughness oriented down the staircase of the steps. Sample A does not.

	Sample A		Sample B		Sample C	
Miscut angles:						
χ	0.40°±0.03°	*M*	0.45°±0.03°	*M*	0.38°±0.03°	*M*
ϕ	0°±5°	*M*	0°±5°	*M*	16°±5°	*M*
Si buffer I:						
Thickness	500 Å	*N*	500 Å	*N*	600 Å	*N*
Growth temperature	750 °C	*N*	750 °C	*N*	500 °C	*N*
Si buffer II:						
Thickness	500 Å	*N*	500 Å	*N*		
Growth temperature	600 °C	*N*	550 °C	*N*		
$Si/Si_{1-x}Ge_x$ Superlattices:						
Number of bilayers	20	*N*	20	*N*	75	*N*
Growth temperature	600 °C	*N*	550 °C	*N*	320 °C	*N*
Si:						
Thickness (d_{Si})	100.0 Å	*N*	100.0 Å	*N*	21.7 Å	*N*
	105.7±0.3 Å	*M*	104.5±0.3 Å	*M*		*M*
Growth rate	1.07 Å/s	*M*	1.71 Å/s	*M*	0.5 Å/s	*M*
$Si_{1-x}Ge_x$:						
Thickness (d_{alloy})	25.0 Å	*N*	25.0 Å	*N*	2.8 Å	*N*
	19.2±0.3 Å	*M*	19.3±0.3 Å	*M*		
x	0.3	*N*	0.5	*N*	1	*N*
	0.25±0.02	*M*	0.45±0.02	*M*		
Vertical strain	1.8±0.15%	*M*	3.2±0.15%	*M*		
Growth rate	0.82 Å/s	*M*	0.82 Å/s	*M*	0.06 Å/s	*M*

again deposited first.

To illustrate the main results of our study, we focus in this paper on three samples (samples A, B, and C) and their companion samples (i.e., samples that have identical nominal structures except for different numbers of bilayers). Table I lists the structures and growth conditions of the samples. Samples A and B are taken from the same place (i.e., same number of bilayers) in two different wafers that were grown to achieve different Ge concentrations in the alloy layers. Sample A has about half the Ge concentration of sample B. Sample C has very thin layers, very low growth rates, and pure Ge in one layer of each layer pair.

B. Characterization techniques

Surface morphology (i.e., the growth front morphology) of the samples is investigated using atomic-force microscopy. These measurements are performed in air using a Digital Instruments Nanoscope III AFM equipped with a 12-μm xyz scanner. Commercially available AFM cantilevers with silicon nitride tips were used. The instrument is calibrated by using mica on which atomic resolution is achieved. The images were taken with a resolution of 512×512 pixels.

X-ray diffraction is used to probe quantitatively several features of the multilayer films and the substrate on which they are grown. These include, for the substrate, miscut from the precise (001) orientation both in polar angle χ and azimuth angle ϕ and, for the film, layer thicknesses of both layers, Ge concentration in the alloy layer, existence and degree of vertical correlation of roughness, roughness anisotropy, and correlation length of the roughness parallel to the interfaces in any azimuth.

A conventional two-circle x-ray diffractometer and Cu $K\alpha$ radiation are used to measure the distribution of diffracted intensity from the multilayer films. The divergence of the radiation source is 0.03° in the diffraction plane. Both the sample and detector can be rotated independently to an accuracy better than 0.01°. The sample, located 21 cm away from the radiation source, is mounted with its surface normal lying in the diffraction plane. The detector, located 21 cm away from the sample, consists of a 50 μm precision slit, a graphite monochromator, and a NaI scintillation counter. The detector is tuned to detect Cu $K\alpha$ radiation and integrates intensity in the direction perpendicular to the diffraction plane.

To establish the miscut, and therefore step density, on the substrate unambiguously, it is necessary to measure it directly rather than to infer it. A determination of substrate quality can be done with the film already deposited, by carefully measuring a substrate reflection. The substrate miscut is completely defined by two angles χ and ϕ. χ is the polar angle between normals of the sample surface and the substrate (001) planes. ϕ is the azimuthal angle in the (001) plane between the [110] direction and the direction of miscut. After the sample is aligned with respect to the outer-surface (i.e., the grown-film surface) normal using low-angle Bragg peaks, the substrate miscut is determined from the additional angles of rotation (i.e., the ω angle; see Fig. 1) of the sample necessary to optimize the (004) reflection from the Si substrate in the slit detector for at least two different azimuthal mountings of the sample (excluding 180° azimuthal rotation of the sample). In this way, the polar angle of miscut (χ) and the azimuthal direction of miscut with respect to the sample are measured. Combining information about the azimuthal miscut direction with respect to the sample and the crystallographic direction obtained from doing Laue diffraction on the samples, the azimuthal angle of miscut (ϕ) with respect to the [110] direction is determined. Because the total thickness of the Si buffer layers and the superlattices is much smaller than the penetration depth of Cu $K\alpha$ radiation, the substrate miscut measurements are not affected by the presence of these layers. The precision of the polar-angle (χ) and azimuthal-angle (ϕ) measurements is $\pm0.03°$ and $\pm5°$, respectively. The typical polar miscut angle χ of the substrates is $\sim0.4°$, corresponding on average to a step separation of about 200 Å.

Layer thicknesses are obtained by fitting the intensity distribution along the superlattice rods [i.e., $(\theta,2\theta)$ scans] obtained from low-angle diffraction.[25] The rms values of the total multilayer interfacial roughness averaged over all the layers and the concentration of Ge in the alloy layers are also obtained from the fit. The rms values are upper limits of the averaged total roughness because the fitting assumes interfacial roughness is a Gaussian random variable. The values for samples A and B are 3.9 ± 5 and 4.5 ± 5 Å, respectively. For sample C, the upper limit of the total rms value for the interfacial roughness cannot be obtained using this method because the layers are so thin and the uncertainty in determining the individual-layer thicknesses is larger than the nominal alloy layer

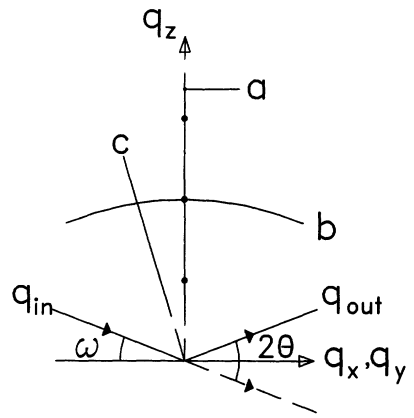

FIG. 1. Schematic diagram of the regions in reciprocal space sampled by a $(\theta,2\theta)$ scan, a transverse scan, and an offset $(\theta,2\theta)$, denoted respectively by *a*, *b*, and *c*. In each case, the scattering vector moves along the lines indicated. In our experiments a slit detector is used that integrates in the direction perpendicular to the diffraction plane, in and out of the plane of the figure. To measure anisotropy in correlated roughness, the figure can be rotated around q_z. The incident and scattered wave vectors are denoted by q_{in} and q_{out}, respectively.

thickness. Because of the tradeoff in the fitting between roughness and concentration, the Ge concentrations obtained in this manner are lower limits of the actual concentrations.

The actual Ge concentration in the alloy layers can also be determined from the amount of vertical separation between atomic planes if the alloy layers are coherently strained. The amount of vertical strain in the alloy layers was extracted from the relative separations between the Si(004) peak (from the substrate) and the superlattice peaks in its vicinity. The Ge concentrations determined in this way are lower limits of the actual values because of the assumption of coherent strain. In calculating the concentration from the measured strain, the ratio of the elastic constants C_{12}/C_{11} is taken to be independent of Ge in the films.[26]

The presence of interfacial roughness in multilayers causes part of the specularly diffracted intensity in x-ray-scattering experiments to be redistributed away from the Bragg peaks into other parts of reciprocal space. If interfacial roughness is correlated[22] (i.e., either perfectly[21] or partially[27–29] copied from interface to interface), then the diffuse-intensity distribution is concentrated in the vicinity of Bragg planes (i.e., planes that are perpendicular to the superlattice rod and pass through the Bragg spots). Conversely, a diffuse-intensity halo in a cut through a Bragg spot indicates the existence of roughness correlated from interface to interface. The detailed shape of this diffuse intensity provides information about the nature of the roughness in the plane of the interfaces; i.e., its rms value, its correlation length, and the existence of preferred wavelengths. In particular, anisotropy in correlated roughness will result in loss of cylindrical symmetry in the diffuse-intensity distribution in the vicinity of Bragg planes. Three types of low-angle x-ray-diffraction scans are used to probe the distribution of diffracted intensity from multilayers. They are $(\theta,2\theta)$ scans, offset-$(\theta,2\theta)$ scans, and transverse scans, as shown in Fig. 1. Typical angles of incidence in these measurements are $0° \leq \theta < 5°$ for Cu $K\alpha$ radiation and the layer thicknesses of our samples.

III. INTERFACIAL ROUGHNESS

In this section we discuss the measurements that demonstrate roughness at interfaces between layers and at the surface of $Si_{1-x}Ge_x/Si$ superlattices. We show how XRD measurements determine roughness correlation and its anisotropy, and show that the correlated roughness anisotropy, when it is present, is oriented in a specific roughness anisotropy, when it is present, is oriented in a specific way with respect to the substrate miscut. We also show that AFM measurements of the surface morphology of the superlattices are consistent with the XRD results: When the XRD diffuse intensity shows that correlated-interfacial-roughness anisotropy is present, the surface shows anisotropic ripples. When XRD indicates no correlated roughness, AFM shows the outer-layer surface roughness to be random and small.

A. X-ray diffraction

Multilayers of $Si_{1-x}Ge_x/Si$ with different superlattice structure or alloy composition can exhibit distinctly different types of diffuse-intensity distributions. Samples A, B, and C described in Table I are chosen to be representative. Figure 2 shows schematic diagrams of the layer structure as well as the measurement geometry for two principal azimuthal orientations. Transverse scans of the samples for these two orientations are shown in Fig. 3. Transverse scans were made at third-, fourth-, and fifth-order Bragg peaks for samples A and B, and at first-and second-order Bragg peaks for sample C. In all cases, they give consistent results. To illustrate that the diffuse peaks in the transverse scans are invariant in reciprocal space at different orders, transverse scans cutting through two different Bragg spots are shown in Fig. 3. The transverse scans have been normalized to the peak intensity after a constant background subtraction followed by an asymmetry correction.[22] The asymmetry correction involves multiplying the intensity by $\sin(\omega)/\sin(\theta)$, where ω is the angle between the incident beam and the sample surface and θ is half the scattering angle. The correction accounts for the fact that, at these small angles, the area of illumination decreases rapidly with increasing angle of incidence, resulting in a lower measured diffuse intensity. The narrow peak at the center (i.e., at $q_x=0$ and $q_y=0$) is the specularly reflected beam; its width is instrument limited. Offset-$(\theta,2\theta)$ scans (Fig. 4) show that the diffuse component is confined mainly to the vicinity of the Bragg planes, indicating that

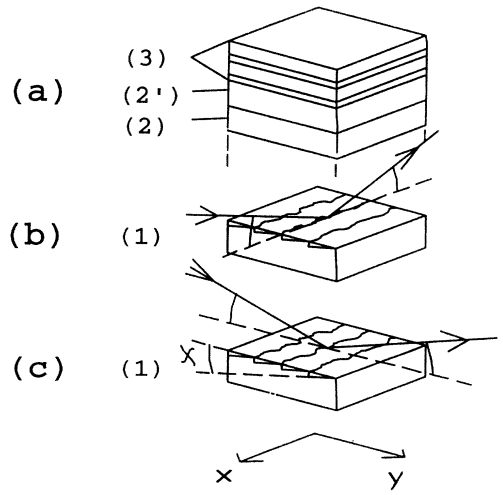

FIG. 2. Schematic diagrams of (a) the structure of $Si_{1-x}Ge_x/Si$ superlattice samples, (b) the x-ray-scattering geometry used in which the sample is oriented such that the plane containing the substrate miscut direction is perpendicular to the diffraction plane, and (c) same as (b) but parallel to the diffraction plane. In the figure, (1), (2) and (2)', and (3) represent the substrate, the buffer layers, and the superlattice, respectively. The top of the superlattice is terminated with a Si layer. In (b) and (c) the superlattice is omitted for clarity. χ is the polar miscut angle. Shown here are cases where the azimuthal miscut angles ϕ are zero. The y axis is defined to lie in the plane containing the miscut direction as shown.

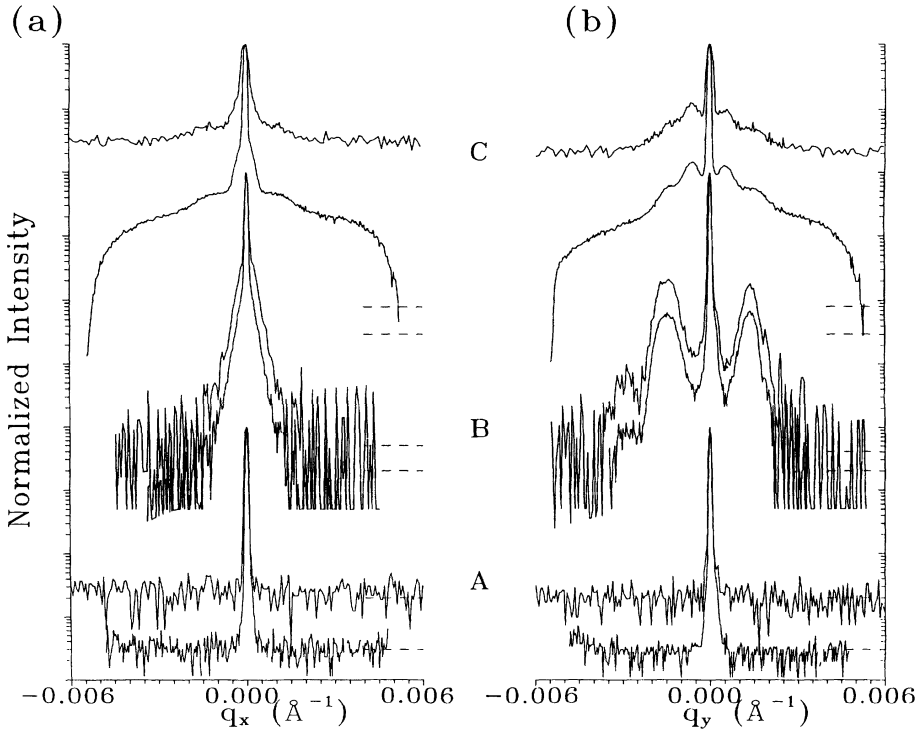

FIG. 3. Transverse scans from three MBE-grown $Si_{1-x}Ge_x/Si$ superlattices (samples A, B, and C). (a) Transverse scans measured with samples oriented azimuthally such that the steps are parallel to the diffraction plane [Fig. 2(b)]. (b) Same, but steps are perpendicular to the diffraction plane (with the incident beam in the descending-step direction of the substrates) [Fig. 2(c)]. The scans from different samples are displaced vertically for clarity. All scans have been normalized to the peak intensity. For samples B and C, normalization is done after background subtraction and asymmetry correction. No such corrections are applied to sample A because the diffuse intensity is practically undetectable. The horizontal dashed lines to the right are the detection limits for the scans, and show in each case the vertical displacement. The fourth- and fifth-order transverse scans are shown for samples A and B, while the first- and second-order transverse scans are shown for sample C. Other orders show the same behavior; in particular, the diffuse peaks for other orders are located at the same q_y.

the roughness is highly correlated vertically from interface to interface.[22,27,28]

The intensity distributions shown in Fig. 3 indicate that the three samples have very different interfacial-roughness correlations. In sample A, which has a relatively low Ge concentration in the alloy layers, diffuse intensity is practically undetectable in transverse and offset $(\theta,2\theta)$ scans, suggesting that it has little correlated roughness. Samples B and C (with higher Ge concentrations) have a strong and azimuthally highly anisotropic diffuse component. The diffuse intensity when the scattering plane lies perpendicular to the steps [i.e., the Fig. 2(c) diffraction geometry, data of Fig. 3(b)], shows well-defined peaks near the specular peak, indicating that the interface morphology is wavy in the miscut direction and correlated from layer to layer. The width (in the q_y direction) of this peak in the diffuse intensity suggests that this waviness consists of a band of wavelengths. Using the diffuse-peak locations at their largest separation from the specular peak as a measure, the mean values of lateral scale lengths of the waviness are 4200±300 Å (with a bandwidth, calculated from the width of the peak measured in the q_y direction, of ≈3000 Å) for sample B and 9500±500 Å (with a bandwidth of ≈6000 Å) for sample C. These values are to be compared with a mean step spacing of ≈200 Å, determined from x-ray-diffraction studies of sample miscut described earlier. In both samples B and C, correlated wavy morphology does not consist of a pure sinusoid because there are higher-order satellites present in the diffuse intensity, as observed in Figs. 3 and 5. The diffuse intensity when the scattering plane lies parallel to the steps [i.e., the Fig. 2(b) diffraction geometry, data in Fig. 3(a)] shows no anisotropic correlated roughness for any of the samples.

So far we have demonstrated (1) the existence of interfacial roughness that has a distinct wavelength (or band of wavelengths) laterally (Fig. 3); (2) an anisotropy of this roughness that appears to be governed by the direction of steps in the vicinal substrate; (3) strong vertical correlation of this roughness, i.e., a high degree of replication from interface to interface (Fig. 4); and (4) an apparent dependence of this interfacial roughness on alloy compo-

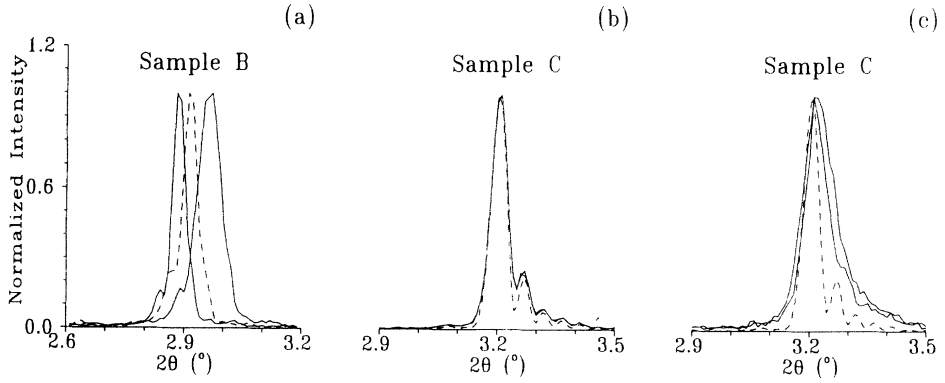

FIG. 4. $(\theta,2\theta)$ scans and offset-$(\theta,2\theta)$ scans (scans *a* and *c*, respectively, in Fig. 1) of samples B and C showing the confinement of diffuse intensity to the vicinity of Bragg planes. The scans are measured with samples oriented azimuthally such that the steps are perpendicular to the diffraction plane [Fig. 2(c)]. In this configuration, the correlated roughness is evident [Fig. 3(b)]. All curves have been normalized to the peak intensity. The dashed curve in every graph is the $(\theta,2\theta)$ scan (i.e., the offset angle is zero). (a) Offset-$(\theta,2\theta)$ scans of sample B around the fourth-order Bragg spot with offset angles at $\pm 0.4°$ (i.e., cutting the fourth-order Bragg plane at $q_y = \pm 1.44 \times 10^{-3}$ Å^{-1}), thus passing directly through the maxima in the diffuse peaks (see Fig. 3). The displacement of the solid curves from the dashed one is explained in Fig. 5. (b) Offset-$(\theta,2\theta)$ scans of sample C around the first-order Bragg spot with offset angles at $\pm 0.15°$ (i.e., cutting the first-order Bragg plane at $q_y = \pm 5.98 \times 10^{-4}$ Å^{-1}), thus passing through the maxima in the diffuse-intensity peaks. (c) Offset- $(\theta,2\theta)$ scans of sample C around the first-order Bragg spot with offset angles at $\pm 0.75°$ (i.e., cutting the first-order Bragg plane at $q_y = \pm 2.99 \times 10^{-3}$ Å^{-1}), thus passing through the isotropic diffuse component. The diffuse-intensity distribution for sample C shows that it has two distinctly different correlated-roughness components: an anisotropic component of longer lateral scale length that is highly correlated between interfaces, and an isotropic component of shorter lateral scale length that is only partially correlated between interfaces.

sition: no correlated roughness when the Ge concentration is low and strongly correlated roughness when the Ge concentration is high.

Additional information about the interfacial morphology can be obtained from the diffuse-intensity distribution I vs q_y and q_z, around one Bragg peak. An example is shown in Fig. 5 for sample B. The maximum values of the peaks at $\pm(q_y)$ in the diffuse intensity lie in planes that are displaced slightly in opposite q_z directions with respect to the Bragg plane. Such a q_z dependence indicates that the wavy morphology is not correlated in the growth direction, but rather that the maxima in the "wave" are displaced laterally so that a ray drawn through them points in a direction slightly off the growth

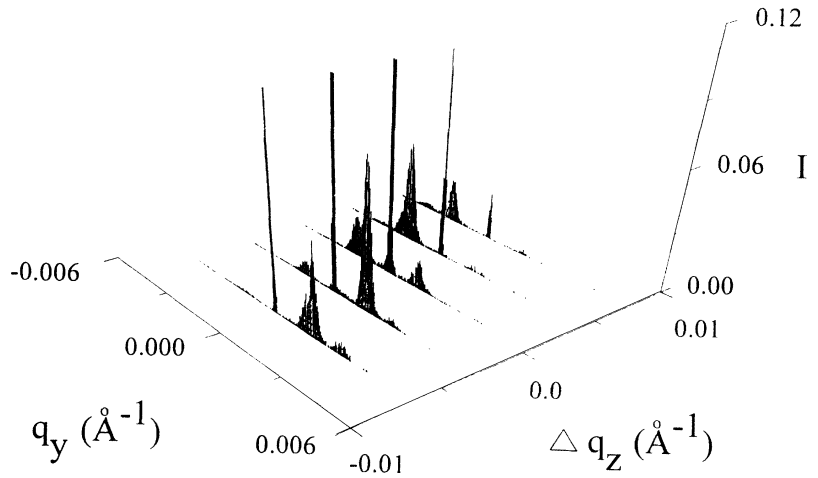

FIG. 5. A set of transverse scans from sample B around the fifth-order Bragg peak. The transverse scans are measured with the sample oriented azimuthally such that the substrate steps are perpendicular to the diffraction plane [Fig. 2(c)]. The scans are normalized to the fifth-order peak intensity. The middle curve cuts through the Bragg peak. Displacement of the diffuse-intensity peaks in the opposite direction along the q_z axis is obvious. The angle between the q_z axis and the line connecting the two main diffuse peaks is $\approx 25°$. The presence of this displacement indicates that the waviness is not correlated in the growth direction but in the direction that is about 25° off the growth direction. The presence of higher-order diffuse satellites indicates that the correlated wavy interfacial morphology is not pure sinusoid.

direction. The angle between the growth direction and the direction of correlation of the waviness is $\approx 25°$. Figure 6 shows a schematic diagram of a possible interfacial morphology for sample B consistent with the XRD measurements. The amplitude of the waviness is obtained from the average total rms roughness [obtained from fitting the $(\theta,2\theta)$ scan] by assuming that all the roughness is correlated.[30] The rationale for this model will be described below. For sample C, there is a significant unequal distribution of the anisotropic diffuse intensity (i.e., the diffuse peak on $+q_y$ is lower than that on $-q_y$) as shown in Fig. 3(b). This shows that the correlated wavy morphology found in sample C is not a symmetry structure (i.e., the wavy morphology does not have reflection symmetry about its center).

B. Atomic-force microscopy

AFM measurements of the superlattice surface morphology are consistent with the x-ray-diffraction results. Samples with alloy layers (types A and B) and with pure Ge layers (type C) have final layers of Si of about 100 and 10 Å, respectively (plus a native oxide). Figure 7 shows typical AFM topographs of samples A and B. The surface of the samples with low Ge concentration [e.g., sample A, Fig. 7(a)] is very smooth and shows no anisotropic surface roughness. The rms value of the corresponding surface roughness is 1.3 ± 0.15 Å (averaged over five independent 10×10 μm^2 images). The images of samples with a Ge concentration above $x\approx0.25$ (e.g., samples B or C) always exhibit a clear anisotropic surface roughness with ripples lying predominantly parallel to the steps of the substrate. For sample B, the rms value of the surface roughness is 3.5 ± 0.5 Å, the average lateral separation of the ripples, determined by Fourier transformation of the AFM images, is 4450 ± 200 Å; and the average height difference between the top and bottom of the ripples is 9 ± 2 Å. The average length of an undisturbed ripple segment is about 3 μm, although sometimes straight ripples with a length of at least 12 μm are observed. As seen in Fig. 7(b), several kinds of deviations from a perfect line pattern are found: the ripples may split or intersect with adjacent ripples, or a further ripple is added causing the adjacent ripples to bend. The ripple height at these defects is decreased compared to that of the undisturbed ones. Higher-resolution images show that the cross section of the ripples is not sinusoid but rather flat on top with "straight" (due to the resolution of AFM) side slopes. On the basis of these results, Fig. 6 should be modified to show that the Si layer growth front is also rough, but to a lesser extent than that of the $Si_{1-x}Ge_x$ layer. For sample C, the rms value of the surface roughness is 5.8 ± 0.5 Å. The surface roughness in sample C has two components: a ripple morphology with a period of about 1 μm superimposed on an isotropic component with a lateral correlation length of only 400 Å.

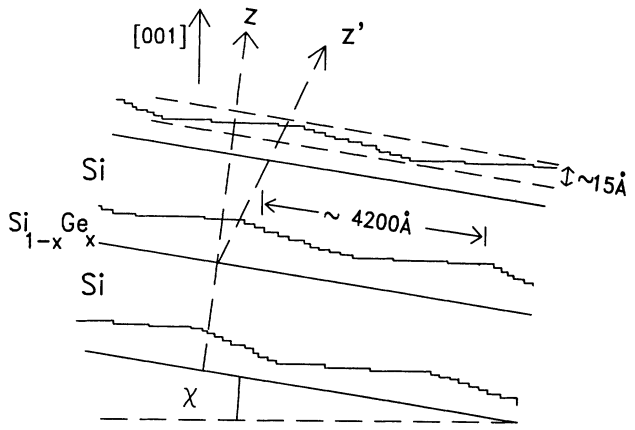

FIG. 6. Schematic diagram of the interface morphology in sample B consistent with XRD measurements. The height difference between the top and bottom of these structures is ≈ 15 Å, based on their shape and a measured rms value of 4.5 Å [obtained from fitting the $(\theta,2\theta)$ scan] (Ref. 25) and the separation of peaks is ≈ 4200 Å. This interface morphology is correlated in a direction z', displaced from the growth direction z. The angle between the growth direction z and the direction of correlation z' is $\approx 25°$. For clarity, the vertical scale is expanded relative to the horizontal scale, the Si layer growth front is shown as smooth, and the steps that are required by the vicinal miscut χ are not explicitly shown.

IV. DISCUSSION

The XRD measurements clearly show that $Si_{1-x}Ge_x$/Si superlattices contain anisotropic correlated interfacial roughness that is oriented in a specific way with respect to the direction of substrate miscut. The AFM measurements corroborate this roughness at the growth front. Moreover, the roughness has a onefold symmetry, i.e., wavy in the direction of substrate miscut and smooth in the orthogonal direction, suggesting a step-catalyzed morphological relaxation. The lateral correlation length of the waviness is, however, many times greater than the average separation of the substrate steps, thus ruling out the possibility that the observed anisotropy is due to vertical correlation of monatomic steps with an average separation determined by the miscut angle of the substrate, as has been suggested.[23,24] Replication of monatomic-height steps in any case cannot produce correlated roughness of the magnitude observed here, even if the length scale matched. (See note added in proof.)

In samples A and B the buffer layers are identical. The fact that sample B shows waviness and A does not rules out the possibility that the anisotropic correlated roughness is due to the bunching of Si steps during the growth of the Si buffer layers, followed by replication of the step bunches by the superlattices.[12] One would have to assume the unlikely scenario that the layers in sample A (which are more like pure Si and thus more likely to replicate the substrate) in fact smoothen the buffer layer step bunches, while those in sample B do not.

The number of bilayers in the superlattices plays a role in the magnitude of anisotropic roughness, but not in its existence. Samples with 10 and 40 bilayers (total superlattice film thickness from ≈ 1250 to ≈ 5000 Å) grown under the same conditions and on substrates with the same miscut as sample A (which has 20 bilayers) show no

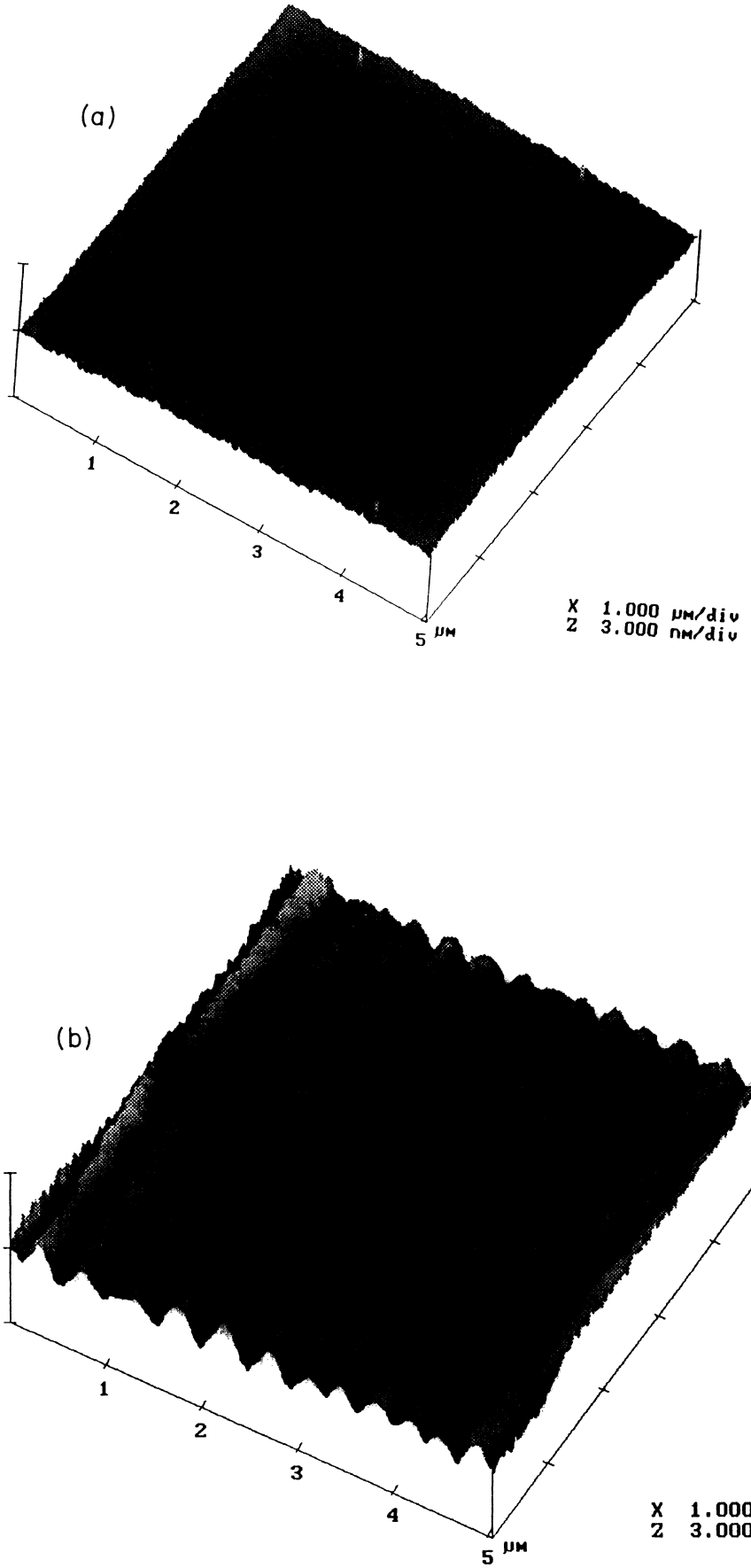

FIG. 7. Surface plots from 5×5 μm^2 AFM images for (a) sample A and (b) sample B. The height scale ranges from -3 to 3 nm. The surface of sample A, except for a few dust particles, is very smooth and shows no anisotropic surface roughness. The rms value of the surface roughness is about 1.3 Å. The surface of sample B clearly exhibits anisotropic surface roughness. Its rms value is about 3.5 Å. The aspect ratio is significantly distorted. The average lateral separation of the ripples is 4450 ± 200 Å. The average height difference between top and bottom of the ripples is 9 ± 2 Å.

detectable correlated roughness. Samples with 10 and 40 bilayers grown under the same conditions and on substrates with the same miscut as sample B (which has 20 bilayers) show the same type of anisotropic correlated roughness as sample B (i.e., wavy in the miscut direction). The mean values of the lateral scale length of the waviness are 4100±300 Å (with a bandwidth of ≈3000 Å) and 5300±300 Å (with a bandwidth of ≈3500 Å) for the 10- and 40-bilayer samples respectively, compared to 4300±300 Å (with a bandwidth of 3000 Å) for the 20-bilayer sample. The upper limits of the rms values of the total roughness averaged over all the layers obtained from fitting the $(\theta,2\theta)$ scans are ≈4.2±0.5 and ≈4.8±0.5 Å for the 10- and 40-bilayer samples, respectively, compared to ≈4.5±0.5 Å for the 20-bilayer sample. The appearance of correlated roughness already in ten-bilayer samples implies that formation of the features that produce anisotropic correlated roughness starts very early in the growth process, and that the vertical correlation is maintained. These results point to the conclusion that the roughness induced in these films is of thermodynamic rather than kinetic origin. Thermodynamic roughness depends only on a balance of free energies, which can be established early in the process. The increase in the rms values for greater layers numbers implies that layers near the top of the stack are rougher. This is confirmed by the AFM measurements, which exhibit a significant increase in average ripple height of the surface with increasing bilayer number.

Samples of type A, which have a low Ge content, show no anisotropic correlated roughness, suggesting that a minimum concentration of Ge is required to produce the correlated wavy morphology. Sample types A and B differ slightly in their growth temperatures; if, as our data indicate, the morphology is thermodynamically controlled, the temperature difference is not a factor. Our results then imply that Ge concentration is the crucial factor in the formation of the anisotropic correlated roughness, something that should be no surprise, as Ge concentration affects strain energy. Sample C, which has a very high Ge concentration but very thin Ge layers, also shows anisotropic correlated roughness. The length scales of the roughness in samples B and C cannot, unfortunately, be directly compared, because of the differences in the layer thicknesses.

At present, no complete explanation exists for the formation of the waviness and especially its anisotropy. Wavy interfaces in $Si_{1-x}Ge_x$/Si superlattices have been observed by others.[12,13,23,24,31] In $Si_{0.5}Ge_{0.5}$/Si superlattices grown by MBE on Si(001), smooth $Si_{0.5}Ge_{0.5}$-on-Si interfaces and wavy Si-on-$Si_{0.5}Ge_{0.5}$ interfaces were observed at high growth temperature, and their formation was attributed to the strain present in the film.[13] The waviness was vertically correlated, but no correlation to possible substrate miscut was reported. In other studies of films grown by chemical-vapor deposition, $Si_{1-x}Ge_x$-on-Si interfaces showed domains of ripples with three different orientations. Two of the sets of ripples were oriented close to the two equivalent ⟨100⟩ directions, and one set was oriented in the [110] miscut direction.[12,31] The two equivalent sets were attributed to strain relaxation, and the latter set of ripples was attributed to substrate step bunching during buffer layer growth.

It seems certain that waviness is related to stress caused by the Ge in the alloy layer. Whenever stress is present, a stress term in the free energy provides an additional driving force for modifying the morphology.[32] We speculate that in order to relax or partially relax the strain in the alloy layers, the system forces extra steps or step bunches. That, by itself, does not provide an explanation for orienting the waviness. In the absence of symmetry breaking, there should be at least two equivalent directions for stress relaxation. Steps in the substrate clearly provide a symmetry breaking but they are much closer together than the wavelength of the interface roughness. As we have shown, substrate steps do not bunch to provide a template of the correct size. Nevertheless the substrate steps apparently serve to orient the morphology of the SiGe film. Local strain fields that are associated with Si steps can cause this effect; the process must be energetically less costly than the random formation of step bunches.[33–36]

Let us consider that the $Si_{1-x}Ge_x$ layer simply uses existing steps in the substrate (due to vicinal miscut) and bunches them in a certain way to relieve strain. By using different rules to bunch these steps, different interfacial morphology can be formed. If all the steps for a $\chi=0.4°$ substrate miscut bunch to form a triangular periodic structure with a (001) face and a (110) face [i.e., a right triangle, Fig. 8(a)] and a wavelength of 4500 Å, then this morphology has a height of 30 Å with a rms value of 8.6 Å. This limiting morphology will give rise to a difference

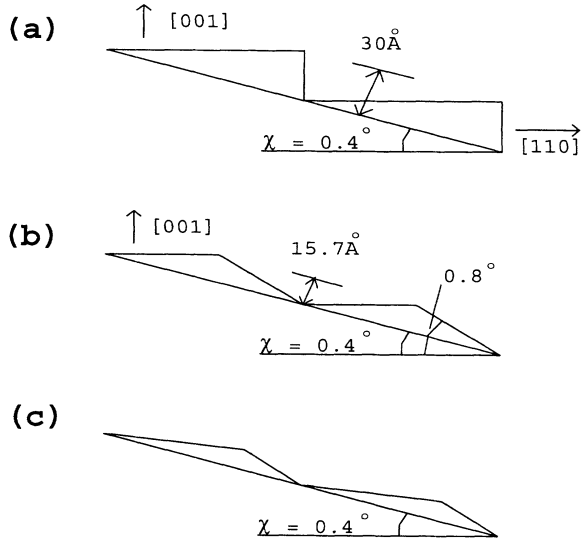

FIG. 8. Schematic diagrams of wavy interfacial morphology formed by bunching existing substrate steps using different rules. (a) Steps bunch to form a periodic triangular structure with (001) and (110) faces. (b) Steps bunch to form a (001) face while simultaneously achieving equal face area on both sides of the triangle. (c) Intermediate case. Interfacial morphologies shown in (b) and (c) are appropriate for samples B and C, respectively.

in the diffuse-intensity distribution in the $-q_y$ region relative to the $+q_y$ region in comparison to the experiment, and a specular intensity that falls off too rapidly with increasing q_z in comparison to the experiment for all samples we have investigated. If the $Si_{1-x}Ge_x$ layer bunches steps in such a way that the triangular periodic structure has a (001) face on one side of the triangle but has equal face areas on both sides of the triangle [Fig. 8(b)], the resulting morphology has a height of 15.7 Å with a rms value of 4.5 Å. For this inclination, the other face of the triangle forms an angle of 0.8° with the (001) plane. Such a morphology and closely related ones with some asymmetry [Fig. 8(c)] seem plausible for sample B. For sample C, because the laterally periodic structure has no reflection symmetry about its center, a plausible structure is one that has some asymmetry [Fig. 8(c)]. In general, if the structure lacks reflection symmetry, it does so by making the "downhill" face shorter as shown in Fig. 8(c).

How does a *correlation* in the interfacial morphology occur? After all, it is not enough that each alloy layer produce step bunches to relieve strain; it is also necessary that these step bunches show some degree of correlation from interface to interface. The Si layers, because their strain is in the opposite direction, would attempt to return the system to the substrate morphology. However, the strain field in the Si layers may be inhomogeneous: because of the multipole field associated with steps, strain in the Si layers located on a step bunch in the alloy layer may be different from that located on a flat terrace in the alloy layer. Where the steps are close, there are two contributions to the strain in the Si layer: one is the lattice mismatch of 4% between Si and Ge, and the other the presence of the steps. On a flat terrace of the alloy layer the strain in a Si layer has only a component due to lattice mismatch. Even though the Si layer has tended to smooth the morphology, the subsequent $Si_{1-x}Ge_x$ layer may now experience an inhomogeneous strain field on the Si spacer layer, leading to some vertical correlation of the regions in which the steps are closer. The implication of this reasoning is that thicker Si layers will allow less correlation in the interfacial roughness, as the strain inhomogeneity due to the alloy layer below weakens with increasing Si-layer thickness. The wavy alloy layer morphology will still form, but with no correlation to that in the alloy layers below. In other words, multilayers with thick Si spacers (or, conversely, too low a Ge concentration in the alloy layer for the Si-layer thickness) may still have interfacial roughness, but with no correlation between the features from layer to layer. We have initial confirmation of this speculation. In any case the two types of interfaces will have different roughness, the Si layer being the smoother, as has been observed in TEM studies.[13] Unfortunately at this time we do not have data on a wide enough range in Si spacer layer thicknesses and in Ge concentration in the alloy to demonstrate at what set of parameters the correlation disappears.

V. SUMMARY

We have observed an interfacial roughness correlation in $Si_{1-x}Ge_x$/Si superlattices that differs as the alloy composition is changed. The vertically correlated interfacial roughness is found to be highly anisotropic and oriented with respect to the substrate miscut, implying that the substrate steps catalyze the formation of the morphology. The lateral length scale of this waviness is many times greater than the average separation of the substrate steps and is therefore not simply a replication of these steps. The formation of step bunches already in the substrate buffer layer can be excluded as the source of the interfacial-roughness correlation. XRD and AFM measurements provide a coherent picture. We present a model for the interfacial morphology and its correlation that is consistent with the measurements and involve anisotropic stress relaxation as the driving force.

Note added in proof. Since this paper went to press, we have measured the surface roughness of buffer layers before the multilayer was deposited and confirmed that steps do not bunch in the buffer layer itself.

ACKNOWLEDGMENTS

We would like to acknowledge useful discussions with X. Chen, D. E. Savage, F. Wu, and Z. Y. Zhang. We would like to thank G. E. Crook and K. J. Wade for the use of their QC-1 x-ray-diffraction system in some of the high-angle diffraction measurements. One of us (C.T.) acknowledges support by the German Academic Exchange Service. This work was supported by NSF, Electronic Materials Program, Grant No. DMR 92-01856.

[1]R. P. G. Karunasiri, J. S. Park, and K. L. Wang, Appl. Phys. Lett. **59**, 2588 (1991).

[2]G. L. Patton, J. H. Comfort, B. S. Meyerson, E. F. Crabbé, G. J. Scilla, E. de Frésart, J. M. C. Stork, J. Y. C. Sun, D. L. Harame, and J. N. Burghartz, IEEE Electron. Device Lett. **11**, 171 (1990).

[3]J. A. Venables, G. D. T. Spiller, and M. Hanbücken, Rep. Prog. Phys. **47**, 399 (1984).

[4]A. Ourmazd and J. C. Bean, Phys. Rev. Lett. **55**, 765 (1985).

[5]F. K. LeGoues, V. P. Kesan, and S. S. Iyer, Phys. Rev. Lett. **64**, 40 (1990).

[6]V. P. Kesan, F. K. LeGoues, and S. S. Iyer, Phys. Rev. B **46**, 1576 (1992).

[7]P. C. Zalm, G. F. A. van de Walle, D. J. Gravesteijn, and A. A. van Gorkum, Appl. Phys. Lett. **55**, 2520 (1989).

[8]B. Y. Tsaur, M. W. Geis, J. C. C. Fan, and R. P. Gale, Appl. Phys. Lett. **38**, 779 (1981).

[9]Y. W. Mo, D. E. Savage, B. S. Swartzentruber, and M. G. Lagally, Phys. Rev. Lett. **65**, 1020 (1990).

[10]J. C. Bean, L. C. Feldman, A. T. Fiory, S. Nakahara, and I. K. Robinson, J. Vac. Sci. Technol. A **2**, 436 (1984).

[11]*Silicon-Molecular Beam Epitaxy,* edited by E. Kasper and J. C. Bean (Chemical Rubber, Boca Raton, 1988), Vol. II, p. 91.

[12]D. J. Robbins, A. G. Cullis, and A. J. Pidduck, J. Vac. Sci.

Technol. B **9**, 2048 (1991).
[13]T. S. Kusan and S. S. Iyer, Appl. Phys. Lett. **59**, 2242 (1991).
[14]For recent reviews on various aspects of growth kinetics in atomistic deposition, see *Kinetics of Ordering and Growth at Surfaces,* edited by M. G. Lagally (Plenum, New York, 1990).
[15]See *Surface Disordering: Growth, Roughening and Phase Transitions,* edited by R. Jullien, J. Kertész, P. Meakin, and D. E. Wolf (Nova Science, Commack, NY, 1993).
[16]Y. H. Xie, Don Monroe, E. A. Fitzgerald, P. J. Silverman, F. A. Thiel, and G. P. Watson, Appl. Phys. Lett. **63**, 2263 (1993).
[17]J. M. Vandenberg, J. C. Bean, R. A. Hamm, and R. Hull, Appl. Phys. Lett. **52**, 1152 (1988).
[18]J.-M. Baribeau, Appl. Phys. Lett. **57**, 1748 (1990).
[19]S. S. Iyer, J. C. Tsang, M. W. Copel, P. R. Pukite, and R. M. Tromp, Appl. Phys. Lett. **54**, 219 (1989).
[20]D. E. Jesson, S. J. Pennycook, and J.-M. Baribeau, Phys. Rev. Lett. **66**,750 (1991).
[21]Y. H. Phang, D. E. Savage, T. F. Kuech, M. G. Lagally, J. S. Park, and K. L. Wang, Appl. Phys. Lett. **60**, 2985 (1992).
[22]D. E. Savage, J. Kleiner, N. Schimke, Y. H. Phang, T. Jankowski, J. Jacobs, R. Kariotis, and M. G. Lagally, J. Appl. Phys. **69**, 1411 (1991).
[23]R. L. Headrick and J.-M. Baribeau, Phys. Rev. B **48**, 9174 (1993).
[24]R. L. Headrick and J.-M. Baribeau, J. Vac. Sci. Technol. B **11**, 1514 (1993).
[25]B. G. Peterson, L. V. Knight, and H. K. Pew, Proc. SPIE **563**, 328 (1985).
[26]E. Bugiel and P. Zaumseil, Appl. Phys. Lett. **62**, 2051 (1993).
[27]D. G. Stearns, J. Appl. Phys. **71**, 4286 (1992).
[28]Y. H. Phang, R. Kariotis, D. E. Savage, and M. G. Lagally, J. Appl. Phys. **72**, 4627 (1992).
[29]Y. H. Phang, D. E. Savage, R. Kariotis, and M. G. Lagally, J. Appl. Phys. **74**, 3181 (1993).
[30]The relationship between the mean square value (σ^2) and the amplitude (A) of a triangular wave is $\sigma^2 = A^2/3$.
[31]A. G. Cullis, D. J. Robbins, A. J. Pidduck, and P. W. Smith, J. Cryst. Growth **123**, 333 (1992).
[32]X. Srolovitz, Acta Metallogr. **37**, 621 (1989).
[33]O. L. Alerhand, D. Vanderbilt, R. D. Meade, and J. D. Joannopoulos, Phys. Rev. Lett. **61**, 1973 (1988).
[34]F. K. Men, W. E. Packard, and M. B. Webb, Phys. Rev. Lett. **61**, 2469 (1988).
[35]R. M. Tromp and M. C. Reuter, Phys. Rev. Lett. **68**, 820 (1992).
[36]J. Tersoff and E. Pehlke, Phys. Rev. Lett. **68**, 816 (1992).

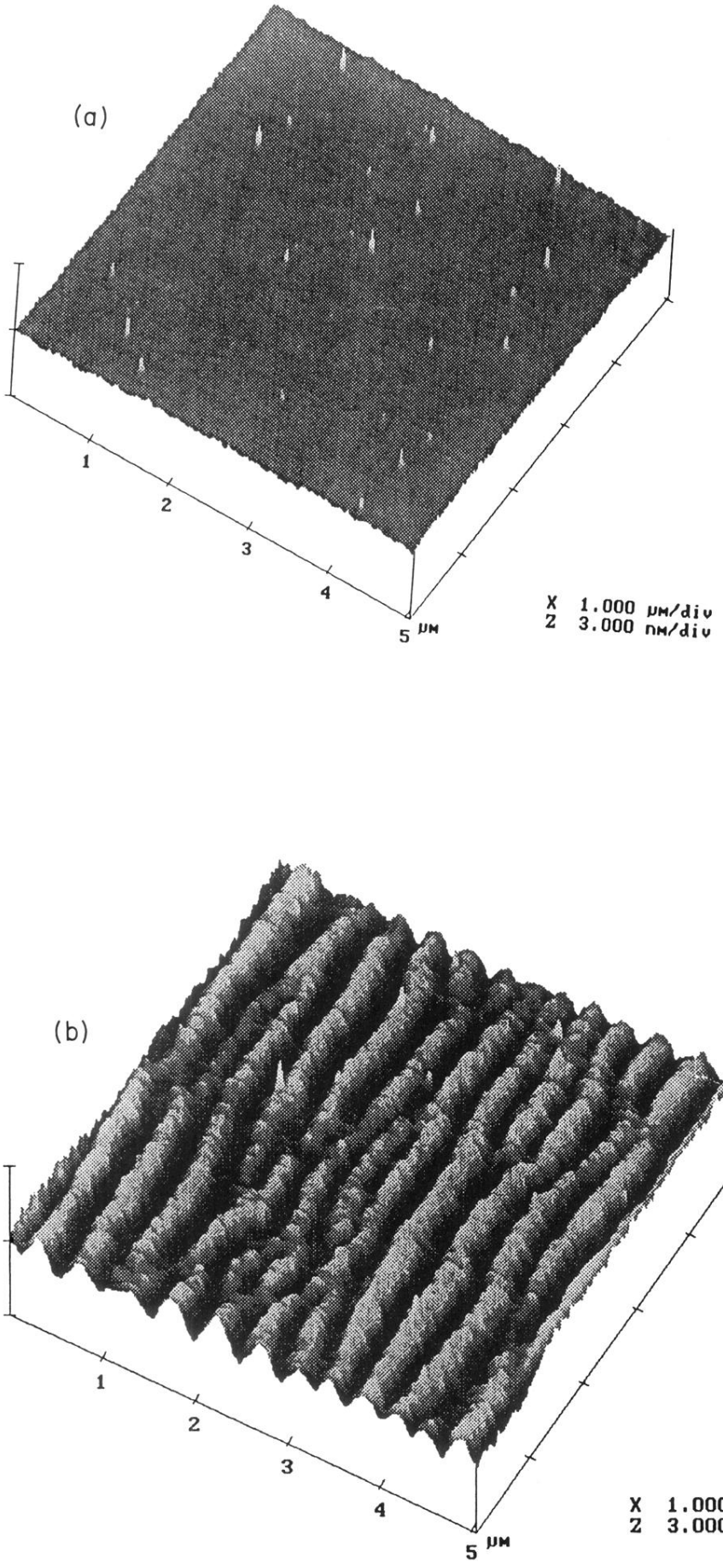

FIG. 7. Surface plots from 5×5 μm^2 AFM images for (a) sample A and (b) sample B. The height scale ranges from -3 to 3 nm. The surface of sample A, except for a few dust particles, is very smooth and shows no anisotropic surface roughness. The rms value of the surface roughness is about 1.3 Å. The surface of sample B clearly exhibits anisotropic surface roughness. Its rms value is about 3.5 Å. The aspect ratio is significantly distorted. The average lateral separation of the ripples is 4450 ± 200 Å. The average height difference between top and bottom of the ripples is 9 ± 2 Å.